C-terminal truncation of α-synuclein alters DNA structure from extension to compaction

Biochemical and Biophysical Research Communications 568 (2021) 43–47

Contents lists available at ScienceDirect

Biochemical and Biophysical Research Communications

journal homepage: www.elsevier.com/locate/ybbrc

C-terminal truncation of α-synuclein alters DNA structure from extension to compaction

Kai Jiang, Sandra Rocha, Ranjeet Kumar, Fredrik Westerlund**, Pernilla Wittung-Stafshede*

Department of Biology and Biological Engineering, Chalmers University of Technology, 412 96, Gothenburg, Sweden

ARTICLE INFO

Article history:
Received 25 May 2021
Accepted 15 June 2021

Keywords:
Nanofluidic channel
α-synuclein
DNA-protein binding
Atomic force microscopy
Single-molecule studies

ABSTRACT

Parkinson's disease (PD) is linked to aggregation of the protein α-synuclein (aS) into amyloid fibers. aS is proposed to regulate synaptic activity and may also play a role in gene regulation via interaction with DNA in the cell nucleus. Here, we address the role of the negatively-charged C-terminus in the interaction between aS and DNA using single-molecule techniques. Using nanofluidic channels, we demonstrate that truncation of the C-terminus of aS induces differential effects on DNA depending on the extent of the truncation. The DNA extension increases for full-length aS and the (1–119)aS variant, but decreases about 25% upon binding to the (1–97)aS variant. Atomic force microscopy imaging showed full protein coverage of the DNA at high aS concentration. The characterization of biophysical properties of DNA when in complex with aS variants may provide important insights into the role of such interactions in PD, especially since C-terminal aS truncations have been found in clinical samples from PD patients.

1. Introduction

Parkinson's disease (PD) is a neurodegenerative disease that is estimated to affect 2% of the population older than 60 years. The main component of the intracellular inclusions (Lewy bodies and neurites) found in the brain of PD patients is α-synuclein (aS) protein in an aggregated form (amyloids) [1,2]. The protein is present mainly at synaptic terminals of the central nervous system [3,4] and is proposed to modulate neurotransmitter vesicle recycling [5–7]. The protein is monomeric at physiological conditions, but can aggregate into amyloid fibrils at pathological conditions, resulting in deposits as well as neuronal cell death. Mostly overlooked, aS is also present in the cell nucleus, which appears to be regulated by different factors, including post-translational modifications [8,9]. aS protein positioned in the nucleus can modulate the transcription level of a master mitochondrial transcription activator called PGC1alpha [10], and aS may also affect repair of DNA [11]. When oxidized and bound to chromatin, aS is able to promote double-strand breaks in DNA and thereby induce cell death [12]. Since aS's physiological function(s) in the nucleus is not known, and whether aS binding to DNA is related to PD initiation, more investigations of aS interacting with DNA are needed.

We recently used nanofluidic channels to investigate how aS binding alters the physical properties of DNA [13]. Nanofluidic channels allow stretching of single DNA molecules by confinement and are perfectly suited for studying how proteins affect the physical properties of DNA [14]. We demonstrated that aS binding to DNA increases the persistence length of DNA [13]. The DNA-protein interaction appears driven by electrostatics and, since DNA is negatively charged, the interaction with the positively charged N-terminal domain of aS will determine the binding to DNA. The sequence of aS can be divided into three domains [15]: the N-terminal region, rich in positively charged residues (12 of a total of 16 positively charged residues) [15,16], the non-amyloid-β component (NAC) domain (residues 61–95), which forms the core of the amyloid fibril [4], and the C-terminus, which is rich in negatively charged residues (15 of a total of 24 negatively charged residues) and is proposed to be involved in protein-protein interactions (Fig. 1). C-terminal truncated variants are more prone to aggregation than full-length aS [17–21]. Importantly, C-terminal truncated variants of aS are found in the brain of both patients with PD and healthy individuals [22,23].

To address the role of C-terminal truncations on aS interaction with DNA, and based on our previous study [13], we applied the

* Corresponding author.
** Corresponding author.;
E-mail addresses: fredrik.westerlund@chalmers.se (F. Westerlund), pernilla.wittung@chalmers.se (P. Wittung-Stafshede).

https://doi.org/10.1016/j.bbrc.2021.06.059

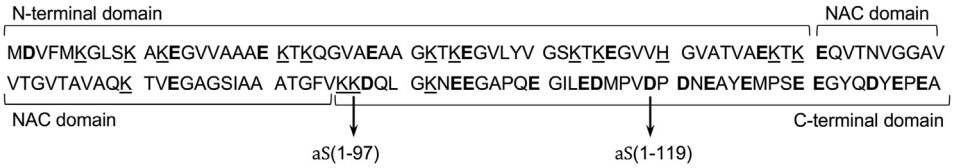

Fig. 1. *AS sequence with the three domains and the positions of the C-terminal truncations studied here marked.* The N-terminal (membrane-binding) domain, the non-amyloid-β component (NAC) domain, and the C-terminal (acidic) domain are highlighted. Charged residues are shown in bold (negative) or underlined (positive).

nanofluidic channel system to characterize the DNA interaction with aS variants truncated in the C-terminal domain and complemented our study with AFM imaging. Our results show that when the complete C-terminus is removed (residues 1–97 remaining in this aS variant), the consequence for the DNA structure upon aS binding is the opposite to that found upon full-length aS binding: DNA is compacted instead of extended.

2. Materials and methods

2.1. Protein expression and purification

Human wild-type (aS (1–140)) and truncated (aS (1–97)) aS variants were heterologously expressed and purified for the experiments as described in Ref. [24]. In addition, C-terminal truncated variant, aS (1–119) was expressed and purified. In short, a pET-21a plasmid with the aS (1–119) gene was transformed into BL21 (DE3) (Novagen) cells. The bacteria were first grown to an OD_{600} of 0.6 in Luria broth (LB) containing 100 μg/ml carbenicillin at 37 °C and then induced with 1 mM IPTG (isopropyl β-D-1-thiogalactopyranoside) and grown overnight at 20 °C post induction. The cells were harvested and lysed by sonication on an ice bath in 20 mM Tris-HCl buffer pH 8.0 in the presence of a protease inhibitor cocktail (Roche). The lysate was then heat treated at 90 °C in a water bath for 10 min followed by centrifugation at 15 000g for 30 min. The supernatant was then filtered through a 0.2 μm filter and loaded on a pre-equilibrated 5 ml HiTrap Q FF anion exchange column (GE Healthcare). The protein was eluted by a linear gradient with 1 M NaCl in 20 mM Tris-HCl buffer pH 8.0. The eluted protein was run on a 4–12% SDS-PAGE and fractions containing the protein of interest were pooled and concentrated with Amicon Ultra-15 10K centrifugal filter units (Millipore). The concentrated protein was loaded and retrieved from a pre-equilibrated Hiload 16/600 Superdex 75 pg column (GE Healthcare) with 20 mM Tris-sulfate buffer pH 7.4.

Sample purity was confirmed for all aS variants by a single band on SDS-PAGE gel, a single elution peak in size exclusion chromatography, and by mass spectrometry. Fractions containing pure protein were pooled and snap frozen in liquid nitrogen and stored at −80 °C. The protein concentration was determined using $\varepsilon_{280} = 5960\ M^{-1}\ cm^{-1}$ for aS (1–140), and $1490\ M^{-1}\ cm^{-1}$ for aS (1–97) and aS (1–119).

2.2. Amyloid formation kinetics

The proteins were gel filtered using a superdex 75, 10/300 GL prepacked column and eluted with Tris-EDTA buffer solution pH 7.4 (10 mM Tris-HCl, 1 mM EDTA, Sigma Aldrich) prior to the aggregation kinetic measurements. A volume of 50 μl/well of each sample with or without 150 mM NaCl was incubated in non-binding polystyrene 96-well half-area plates with clear bottom (Corning Life Sciences) at 37 °C in the presence of a borosilicate glass bead of 2 mm. Thioflavin T fluorescence was monitored every 20 min, with agitation 5 min before each measurement, using a microplate reader (FLUOstar Optima, BMG Labtech) with excitation wavelength set at 440 nm and emission wavelength at 480 nm.

2.3. Nanofluidics

DNA from phage lambda (λ-DNA, Roche) was mixed with each aS variant and then stained with YOYO-1 (Invitrogen) at a ratio of 1 dye molecule per 25 base pairs in 1 × TE (10 mM Tris; 1 mM EDTA). The mixture was incubated at 4 °C for at least 2 h. The complexes were introduced into the nanofluidic system and equilibrated for 60 s before image capture. The DNA concentration was 5 μM (basepairs) in all samples. 3% (v/v) β-mercaptoethanol (Sigma–Aldrich) was added as an oxygen scavenger to suppress oxygen radical induced photo-damage of the DNA. The single DNA molecule experiments were performed in nanochannels with dimensions of 150 × 100 nm^2. The devices were fabricated using advanced nanofabrication described elsewhere [25]. The channel system consists of a pair of feeding channels (micron sized), spanned by a set of parallel nanochannels (schematic illustration in Fig. 3A). The sample was loaded into the channel system from one of the four reservoirs that are connected to the feeding channels and moved into the nanochannels by pressure driven (N_2) flow. To avoid non-specific binding of protein to the negatively charged channel walls, the channels were coated with a lipid bilayer comprising 99% 1-palmitoyl-2-oleoyl-*sn*-glycero-3-phosphocholine (POPC, Avanti) and 1% N-(fluorescein-5-thiocarbamoyl)-1,2-dihexadecano-yl-*sn*-Glycero-3-phosphoethanolamine, triethyl ammonium salt (fluorescein-DHPE, Invitrogen) prior to the experiment. The coating procedure is described elsewhere [26].

The DNA and DNA-protein complexes were imaged using an epi-fluorescence microscope (Zeiss AxioObserver.Z1) equipped with a Photometrics Evolve EMCCD camera, a 63X oil immersion TIRF objective (NA = 1.46) and a 1.6X optovar from Zeiss. Using the microscopy imaging software ZEN, 100 subsequent images were recorded with an exposure time of 100 ms. Data analysis was performed using a custom-written MATLAB-based software as described elsewhere [27].

2.4. Atomic force microscopy (AFM)

NoLimits 1000 bp DNA (ThermoFisher Scientific) was mixed with aS variants at a basepair:protein molar ratio of 15 and the samples were incubated at 4 °C for at least 2 h. 10 μl of each aS-DNA sample was adsorbed on silicon substrates treated as described previously [13]. After 10 min adsorption, the wafer was washed with Milli-Q water and dried using N_2 gas. Samples with bare DNA were prepared on freshly cleaved mica after adding 0.2 mM $MgCl_2$ to 1000 bp DNA (10 min adsorption on mica, wash with Milli-Q, and dried using N_2 gas). AFM images were recorded in air, with a Dimension ICON scanning probe microscope (Bruker) operating in peak force tapping mode (force constant of 1.45–15.1 Nm^{-1}, resonant frequency of 87–230 kHz; scanning rate of 1 Hz). Data analysis was performed with open-source software Gwyddion (http://gwyddion.net/).

3. Results

Since aS binding to DNA is proposed to be governed in part by charge-charge interactions [13], we investigated whether the protein binding was affected by truncation of the aS C-terminal domain, which would remove negatively charged residues that are unfavorable for binding to the negatively charged backbone of the DNA. We studied two C-terminal truncated aS variants: one containing residues 1–97 (aS (1–97)) and another containing residues 1–119 (aS (1–119)), thereby removing 15 and 8 negatively charged residues from the full-length polypeptide, respectively.

First, we tested that the purified aS variants formed amyloids as expected. The aggregation kinetics of the two aS variants and full-length aS (aS (1–140)) were monitored immediately after gel filtration chromatography to ensure that only protein monomers were present at the starting point. The aggregation experiments were performed under agitation in the presence of a glass bead to increase the reproducibility [28]. Sigmoidal aggregation profiles were obtained for all variants (30 μM, 37 °C, pH 7.4) in the presence of 150 mM NaCl with a lag phase of around 8 h for aS (1–140), 6 h for aS (1–119), and 3 h for aS (1–97) (Fig. 2A). Decreasing the ionic strength (thereby enhancing electrostatic effects) significantly slowed down the aggregation rate of aS (1–140) (Fig. 2B), but had no effect on the aggregation of aS (1–97) (Fig. 2C), supporting that the presence of negatively charged residues in the C-terminal domain delays aS (1–140) amyloid fibril formation. Importantly, these experiments showed that aggregation is slow (several hours of lag phase), even at conditions (glass bead and agitation) that favor aggregation. aS incubated without agitation does not aggregate at the conditions used here. Therefore, in the nanofluidic channel experiments, where the samples were mixed without agitation and measurements were performed within 2 h of sample preparation, amyloid formation of the aS variants is not expected.

To investigate individual DNA molecules upon binding of the aS variants, the experimental set up included 48.5 kbp λ-DNA (5 μM base pairs) mixed with a range of aS concentrations (up to 40 μM; providing 8:1 aS-to-base pair ratio at the highest protein concentration). For such mixtures, we determined the extension of individual DNA molecules in nanofluidic channels having a 100 × 150 nm^2 geometry (Fig. 3A). To visualize the DNA, the well-characterized fluorophore YOYO-1 was used: it binds to DNA via intercalation between DNA base pairs [29]. The relative extension R_{II}/L (extension R_{II} normalized to the DNA contour length L) of DNA molecules increased with the protein:base pair ratio for full length aS (1–140) (as reported before [13]) and for aS (1119), but decreased in the case of aS (1–97) (Fig. 3B; examples in Fig. 3C). Importantly, the changes induced by aS variants (~25% compaction by aS (1–97) or ~30% extension by aS (1–140) and aS (1–119)) are minor when

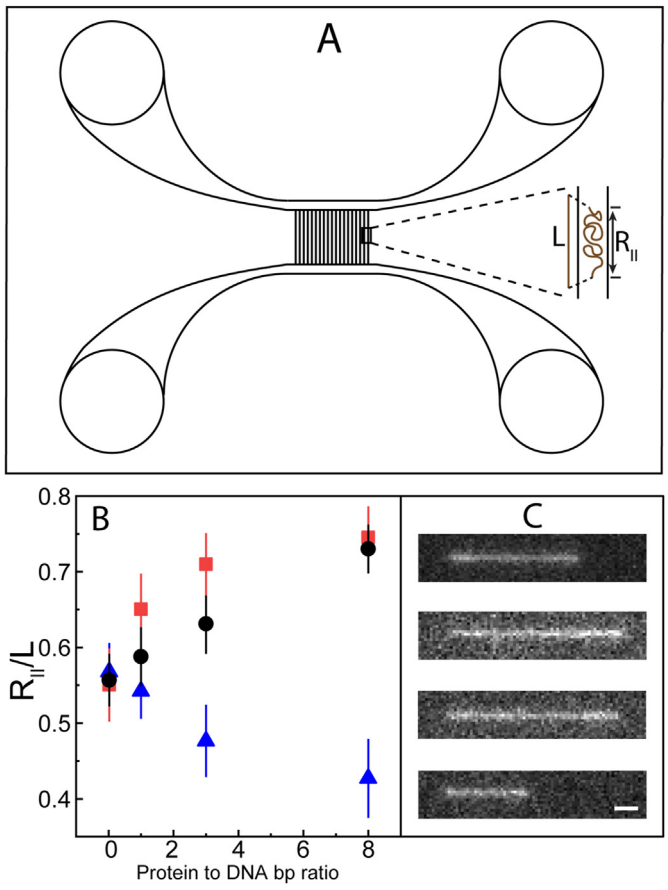

Fig. 3. *Nanofluidic set up and results upon aS addition to DNA.* (**A**) Schematic illustration of the nanofluidic chip design. The channel system comprises pairs of micro-channels, spanned by an array of nanochannels (100 × 150 nm^2). The cartoon shows a DNA moleule confined inside a nanochannel. DNA will be partially stretched along the nanochannel with an extension R_{II} shorter than its contour length L. (**B**) Relative extension R_{II}/L of λ-DNA in the presence of aS (1–140) (●, black), aS (1–119) (■, red) and aS (1–97) (△, blue) in 1 × TE buffer in 150 × 100 nm^2 channels, versus the protein to DNA base pair (bp) ratio. (**C**) Representative fluorescence images of λ-DNA with aS variants. Top to bottom: bare DNA, DNA with aS (1–140), DNA with aS (1–119), and DNA with aS (1–97), each at a protein to base pair ratio of 8:1. The scale bar is 1 μm. (For interpretation of the references to colour in this figure legend, the reader is referred to the Web version of this article.)

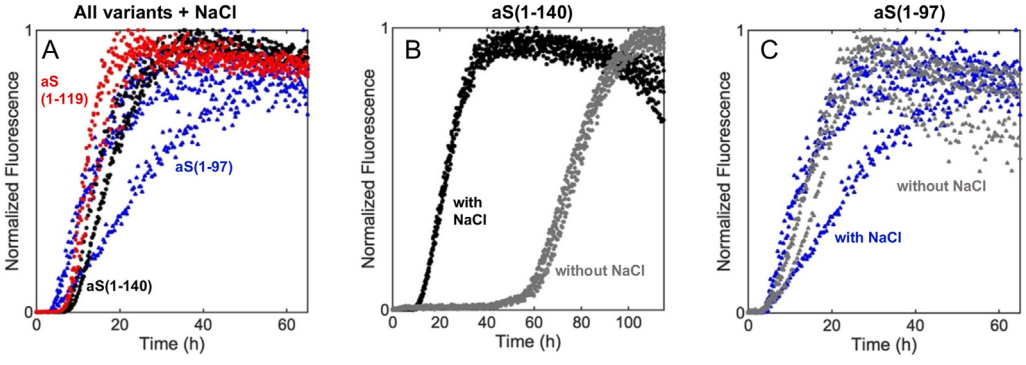

Fig. 2. *Aggregation kinetics of aS variants incubated under agitation in the presence of a glass bead (37°C, pH 7.4).* (**A**) aS (1–140) (●, black), aS (1–119) (■, red) and aS (1–97) (△, blue) samples with 150 mM NaCl. (**B**) aS (1–140) incubated in the absence (gray) and presence of 150 mM NaCl (black); (**C**) aS (1–97) incubated in the absence (gray) and presence (blue) of 150 mM NaCl. Three replicates are shown and the protein concentration was 30 μM. (For interpretation of the references to colour in this figure legend, the reader is referred to the Web version of this article.)

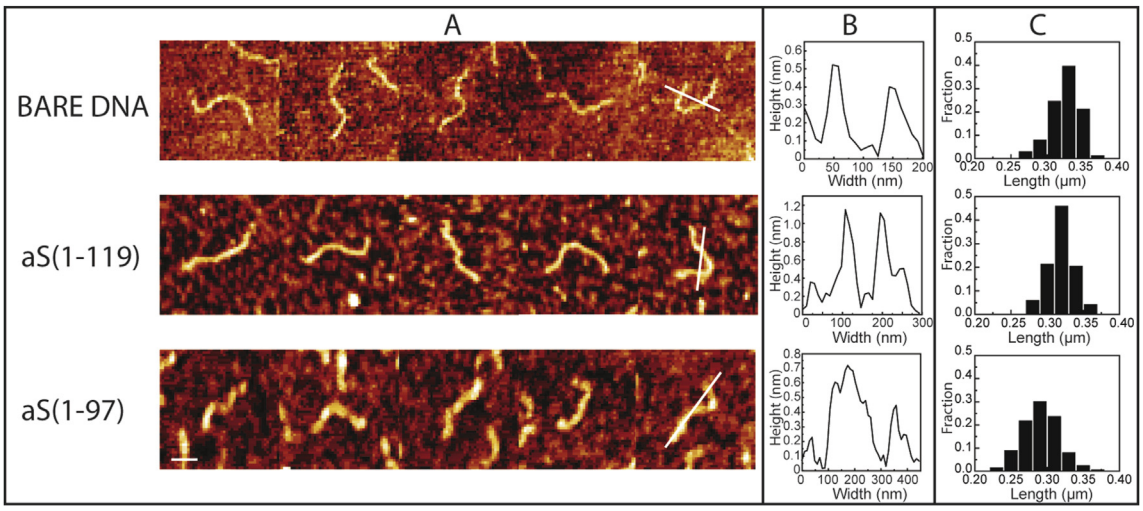

Fig. 4. *AFM analysis of the binding of aS variants to DNA.* (**A**) Tapping mode AFM images of bare DNA (1kbp, 5 μM base pairs) and DNA with aS (1–119) or aS (1–97) at a protein concentration of 15 μM (3:1 protein:DNA). The scale bar is 100 nm. The line in each panel corresponds to the height profile of the molecule shown in (**B**). The corresponding distributions of DNA contour length are shown in (**C**).

compared to other proteins that can induce full compaction of DNA [30,31]. Another observation is that, for all aS variants, it is possible to stain the DNA with YOYO-1 even though the DNA is fully coated with protein, suggesting that binding sites for YOYO-1 are still available on DNA.

As a complement to the nanochannel data, we turned to atomic force micrsocopy (AFM) analysis using shorter DNA (1kbp, 5 μM base pairs) and the aS (1–97) and aS (1–119) variants at a protein:base pair ratio of 3:1 (Fig. 4A). We found that the DNA height increased in the presence of both aS variants, from approximately 0.5 nm for bare DNA to 0.7–1.0 nm in the presence of the protein and the DNA appears to be fully covered by the proteins (Fig. 4B). This is similar to what we found earlier for aS (1–140) [13]. Whereas the DNA contour length did not change upon aS (1–119) binding as compared to bare DNA, the DNA contour length decreased for aS (1–97) (Fig. 4C), which parallels the result of DNA compaction in the nanochannel.

4. Discussion

We here show that C-terminal truncation of aS can induce changes from extension (over 30% DNA length increase for aS (1–140) binding and aS (1–119)) to compaction (more than 20% DNA length decrease for aS (197) binding). Clearly, sufficient removal of negatively charged residues from aS changes the resulting structural consequences for DNA upon protein binding. The most important residues appear to be located between residues 97 and 119 in the sequence. It appears that upon full C-terminal truncation (43 residues), aS behaves as one expects for multivalent cation interactions, which often lead to compaction of DNA. However, we do not observe full compaction of DNA [30,31] suggesting that the aS-DNA interaction is relatively weak, as is also reflected by the high concentration of aS needed to saturate the effect on DNA. The differential result with aS (1–97) reinforces that the interaction between full-length aS and DNA includes other forces, such as hydrophobic and/or specific interactions. For a fully coated DNA it is also possible that protein-protein interactions between peptides next to each other affect the binding. For full length aS we concluded that the increase in DNA extension was due to an increase in DNA persistence length [13] and we propose a similar mechanism for aS (1–119).

Several proteins bind to DNA and affect its structure as a way to modulate activity, such as gene replication and transcription. For example, different bacterial nucleoid proteins (e.g., H-NS, Hfq, and HU) have been shown to specifically compact or extend DNA [32–34]. To better understand the role of aS-DNA interactions in PD, underlying molecular principles of such complexes need to be charcterized. Several proteins and short peptides linked to other amyloidogenic disorders, including Alzheimer's, Amyotrophic lateral sclerosis (ALS) and prion diseases, exhibit nucleic acid binding abilities that may be of functional relevance [35]. Moreover, liquid-liquid phase separated biological systems often involve loosely associated -complexes (involving multivalent often electrostatic interactions) between amyloidogenic proteins and RNA [36,37]. Single DNA molecule techniques, such as the approach used here, may be useful to characterize putative nucleic-acid binding of many other proteins involved in both function and disease.

Declaration of competing interest

The authors declare that they have no known competing financial interests or personal relationships that could have appeared to influence the work reported in this paper.

Acknowledgements

Kai Jiang acknowledges a postdoctoral fellowship from the Wenner-Gren Foundation. PWS (2015–03881 and 2019–03673) and FW (2015–05062 and 2020–03400) acknowledge funding from the Swedish Research Council. PWS also acknowledges funding from the Knut and Alice Wallenberg Foundation. FW also acknowledges funding from the European Research Council in the form of a Consolidator Grant (nanoDNArepair, no. 866238). We thank Dr. Sriram KK for fabricating the nanofluidic channels.

References

[1] M.G. Spillantini, M.L. Schmidt, V.M.Y. Lee, J.Q. Trojanowski, R. Jakes, M. Goedert, alpha-synuclein in Lewy bodies, Nature 388 (1997) 839–840, https://doi.org/10.1038/42166.

[2] K. Wakabayashi, K. Tanji, S. Odagiri, Y. Miki, F. Mori, H. Takahashi, The lewy body in Parkinson's disease and related neurodegenerative disorders, Mol. Neurobiol. 47 (2013) 495–508, https://doi.org/10.1007/s12035-012-8280-y.

[3] L. Maroteaux, J.T. Campanelli, R.H. Scheller, Synuclein: a neuron-specific protein localized to the nucleus and presynaptic nerve terminal, J. Neurosci. 8 (1988) 2804–2815.
[4] A. Iwai, E. Masliah, M. Yoshimoto, N. Ge, L. Flanagan, H.A. de Silva, A. Kittel, T. Saitoh, The precursor protein of non-A beta component of Alzheimer's disease amyloid is a presynaptic protein of the central nervous system, Neuron 14 (1995) 467–475, https://doi.org/10.1016/0896-6273(95)90302-x.
[5] V.M. Nemani, W. Lu, V. Berge, K. Nakamura, B. Onoa, M.K. Lee, F.A. Chaudhry, R.A. Nicoll, R.H. Edwards, Increased expression of alpha-synuclein reduces neurotransmitter release by inhibiting synaptic vesicle reclustering after endocytosis, Neuron 65 (2010) 66–79, https://doi.org/10.1016/j.neuron.2009.12.023.
[6] S.L. Senior, N. Ninkina, R. Deacon, D. Bannerman, V.L. Buchman, S.J. Cragg, R. Wade-Martins, Increased striatal dopamine release and hyperdopaminergic-like behaviour in mice lacking both alpha-synuclein and gamma-synuclein, Eur. J. Neurosci. 27 (2008) 947–957, https://doi.org/10.1111/j.1460-9568.2008.06055.x.
[7] L. Yavich, H. Tanila, S. Vepsalainen, P. Jakala, Role of alpha-synuclein in presynaptic dopamine recruitment, J. Neurosci. 24 (2004) 11165–11170, https://doi.org/10.1523/JNEUROSCI.2559-04.2004.
[8] S. Goncalves, T.F. Outeiro, Assessing the subcellular dynamics of alpha-synuclein using photoactivation microscopy, Mol. Neurobiol. 47 (2013) 1081–1092, https://doi.org/10.1007/s12035-013-8406-x.
[9] R. Pinho, I. Paiva, K.G. Jercic, L. Fonseca-Ornelas, E. Gerhardt, C. Fahlbusch, P. Garcia-Esparcia, C. Kerimoglu, M.A.S. Pavlou, A. Villar-Pique, E. Szego, T. Lopes da Fonseca, F. Odoardi, S. Soeroes, A.C. Rego, W. Fischle, J.C. Schwamborn, T. Meyer, S. Kugler, I. Ferrer, J. Attems, A. Fischer, S. Becker, M. Zweckstetter, F. Borovecki, T.F. Outeiro, Nuclear localization and phosphorylation modulate pathological effects of alpha-synuclein, Hum. Mol. Genet. 28 (2019) 31–50, https://doi.org/10.1093/hmg/ddy326.
[10] A. Siddiqui, S.J. Chinta, J.K. Mallajosyula, S. Rajagopolan, I. Hanson, A. Rane, S. Melov, J.K. Andersen, Selective binding of nuclear alpha-synuclein to the PGC1alpha promoter under conditions of oxidative stress may contribute to losses in mitochondrial function: implications for Parkinson's disease, Free Radic. Biol. Med. 53 (2012) 993–1003, https://doi.org/10.1016/j.freeradbiomed.2012.05.024.
[11] A.J. Schaser, V.R. Osterberg, S.E. Dent, T.L. Stackhouse, C.M. Wakeham, S.W. Boutros, L.J. Weston, N. Owen, T.A. Weissman, E. Luna, J. Raber, K.C. Luk, A.K. McCullough, R.L. Woltjer, V.K. Unni, Alpha-synuclein is a DNA binding protein that modulates DNA repair with implications for Lewy body disorders, Sci. Rep. 9 (2019), 10919, https://doi.org/10.1038/s41598-019-47227-z.
[12] V. Vasquez, J. Mitra, P.M. Hegde, A. Pandey, S. Sengupta, S. Mitra, K.S. Rao, M.L. Hegde, Chromatin-bound oxidized alpha-synuclein causes strand breaks in neuronal genomes in in vitro models of Parkinson's disease, J Alzheimers Dis 60 (2017) S133–S150, https://doi.org/10.3233/JAD-170342.
[13] K. Jiang, S. Rocha, A. Westling, S. Kesarimangalam, K.D. Dorfman, P. Wittung-Stafshede, F. Westerlund, Alpha-synuclein modulates the physical properties of DNA, Chemistry 24 (2018) 15685–15690, https://doi.org/10.1002/chem.201803933.
[14] K. Frykholm, L.K. Nyberg, F. Westerlund, Exploring DNA-protein interactions on the single DNA molecule level using nanofluidic tools, Integr Biol (Camb) 9 (2017) 650–661, https://doi.org/10.1039/c7ib00085e.
[15] L. Breydo, J.W. Wu, V.N. Uversky, Alpha-synuclein misfolding and Parkinson's disease, Biochim. Biophys. Acta 1822 (2012) 261–285, https://doi.org/10.1016/j.bbadis.2011.10.002.
[16] G. Drin, B. Antonny, Amphipathic helices and membrane curvature, FEBS Lett. 584 (2010) 1840–1847, https://doi.org/10.1016/j.febslet.2009.10.022.
[17] W. Hoyer, D. Cherny, V. Subramaniam, T.M. Jovin, Impact of the acidic C-terminal region comprising amino acids 109-140 on alpha-synuclein aggregation in vitro, Biochemistry-Us 43 (2004) 16233–16242, https://doi.org/10.1021/bi048453u.
[18] K. Levitan, D. Chereau, S.I. Cohen, T.P. Knowles, C.M. Dobson, A.L. Fink, J.P. Anderson, J.M. Goldstein, G.L. Millhauser, Conserved C-terminal charge exerts a profound influence on the aggregation rate of alpha-synuclein, J. Mol. Biol. 411 (2011) 329–333, https://doi.org/10.1016/j.jmb.2011.05.046.
[19] C.W. Liu, B.I. Giasson, K.A. Lewis, V.M. Lee, G.N. DeMartino, P.J. Thomas, A precipitating role for truncated alpha-synuclein and the proteasome in alpha-synuclein aggregation - implications for pathogenesis of Parkinson disease, J. Biol. Chem. 280 (2005) 22670–22678, https://doi.org/10.1074/jbc.M501508200.
[20] I.V.J. Murray, B.I. Giasson, S.M. Quinn, V. Koppaka, P.H. Axelsen, H. Ischiropoulos, J.Q. Trojanowski, V.M.Y. Lee, Role of alpha-synuclein carboxy-terminus on fibril formation in vitro, Biochemistry-Us 42 (2003) 8530–8540, https://doi.org/10.1021/bi027363r.
[21] W. Wang, L.T. Nguyen, C. Burlak, F. Chegini, F. Guo, T. Chataway, S. Ju, O.S. Fisher, D.W. Miller, D. Datta, F. Wu, C.X. Wu, A. Landeru, J.A. Wells, M.R. Cookson, M.B. Boxer, C.J. Thomas, W.P. Gai, D. Ringe, G.A. Petsko, Q.Q. Hoang, Caspase-1 causes truncation and aggregation of the Parkinson's disease-associated protein alpha-synuclein, Proc. Natl. Acad. Sci. U. S. A. 113 (2016) 9587–9592, https://doi.org/10.1073/pnas.1610099113.
[22] M. Baba, S. Nakajo, P.H. Tu, T. Tomita, K. Nakaya, V.M.Y. Lee, J.Q. Trojanowski, T. Iwatsubo, Aggregation of alpha-synuclein in Lewy bodies of sporadic Parkinson's disease and dementia with lewy bodies, Am. J. Pathol. 152 (1998) 879–884.
[23] G. Muntane, I. Ferrer, M. Martinez-Vicente, alpha-synuclein phosphorylation and truncation are normal events in the adult human brain, Neuroscience 200 (2012) 106–119, https://doi.org/10.1016/j.neuroscience.2011.10.042.
[24] I. Horvath, T. Werner, R. Kumar, P. Wittung-Stafshede, Copper chaperone blocks amyloid formation via ternary complex, Q. Rev. Biophys. 51 (2018), e6, https://doi.org/10.1017/S0033583518000045.
[25] F. Westerlund, F. Persson, A. Kristensen, J.O. Tegenfeldt, Fluorescence enhancement of single DNA molecules confined in Si/SiO2 nanochannels, Lab Chip 10 (2010) 2049–2051, https://doi.org/10.1039/c004878j.
[26] F. Persson, J. Fritzsche, K.U. Mir, M. Modesti, F. Westerlund, J.O. Tegenfeldt, Lipid-based passivation in nanofluidics, Nano Lett. 12 (2012) 2260–2265, https://doi.org/10.1021/nl204535h.
[27] K. Jiang, N. Humbert, S. Kk, T. Lequeu, Y.L. Lin, Y. Mely, F. Westerlund, Annealing of ssDNA and compaction of dsDNA by the HIV-1 nucleocapsid and Gag proteins visualized using nanofluidic channels, Q. Rev. Biophys. 52 (2019) e2, https://doi.org/10.1017/S0033583518000124.
[28] L. Giehm, N. Lorenzen, D.E. Otzen, Assays for alpha-synuclein aggregation, Methods 53 (2011) 295–305, https://doi.org/10.1016/j.ymeth.2010.12.008.
[29] L. Nyberg, F. Persson, B. Akerman, F. Westerlund, Heterogeneous staining: a tool for studies of how fluorescent dyes affect the physical properties of DNA, Nucleic Acids Res. 41 (2013), e184, https://doi.org/10.1093/nar/gkt755.
[30] K. Jiang, N. Humbert, K.S. K, I. Rouzina, Y. Mely, F. Westerlund, The HIV-1 nucleocapsid chaperone protein forms locally compacted globules on long double-stranded DNA, Nucleic Acids Res. (2021), https://doi.org/10.1093/nar/gkab236.
[31] R. Sharma, S. Kk, E.D. Holmstrom, F. Westerlund, Real-time compaction of nanoconfined DNA by an intrinsically disordered macromolecular counterion, Biochem. Biophys. Res. Commun. 533 (2020) 175–180, https://doi.org/10.1016/j.bbrc.2020.06.051.
[32] D. Guttula, F. Liu, J.A. van Kan, V. Arluison, J.R.C. van der Maarel, Effect of HU protein on the conformation and compaction of DNA in a nanochannel, Soft Matter 14 (2018) 2322–2328, https://doi.org/10.1039/c7sm02118f.
[33] K. Jiang, C. Zhang, D. Guttula, F. Liu, J.A. van Kan, C. Lavelle, K. Kubiak, A. Malabirade, A. Lapp, V. Arluison, J.R. van der Maarel, Effects of Hfq on the conformation and compaction of DNA, Nucleic Acids Res. 43 (2015) 4332–4341, https://doi.org/10.1093/nar/gkv268.
[34] C. Zhang, A. Hernandez-Garcia, K. Jiang, Z. Gong, D. Guttula, S.Y. Ng, P.P. Malar, J.A. van Kan, L. Dai, P.S. Doyle, R. Vries, J.R. van der Maarel, Amplified stretch of bottlebrush-coated DNA in nanofluidic channels, Nucleic Acids Res. 41 (2013), e189, https://doi.org/10.1093/nar/gkt783.
[35] S. Camero, M.J. Benitez, J.S. Jimenez, Anomalous protein-DNA interactions behind neurological disorders, Adv Protein Chem Struct Biol 91 (2013) 37–63, https://doi.org/10.1016/B978-0-12-411637-5.00002-0.
[36] S. Boeynaems, S. Alberti, N.L. Fawzi, T. Mittag, M. Polymenidou, F. Rousseau, J. Schymkowitz, J. Shorter, B. Wolozin, L. Van Den Bosch, P. Tompa, M. Fuxreiter, Protein phase separation: a new phase in cell biology, Trends Cell Biol. 28 (2018) 420–435, https://doi.org/10.1016/j.tcb.2018.02.004.
[37] D.S.W. Protter, R. Parker, Principles and properties of stress granules, Trends Cell Biol. 26 (2016) 668–679, https://doi.org/10.1016/j.tcb.2016.05.004.